

ANALYSIS OF REGIONAL CHARACTERISTICS OF THE ATMOSPHERIC HEAT BALANCE IN THE TOKYO METROPOLITAN AREA IN SUMMER

Ryozo Ooka^{1†}, Taiki Sato², and Shuzo Murakami³

¹ *Institute of Industrial Science, University of Tokyo, 4-6-1 Komaba, Meguro-ku, Tokyo 153-8505, Japan*

² *Taisei Corporation, 1-25-1 Nishi-Shinjuku, Shinjuku-ku, Tokyo 163-0606, Japan*

³ *Keio University, 3-14-1 Hiyoshi Kohoku-ku, Yokohama-shi, Kanagawa-ken 223-8522, Japan*

ABSTRACT

The heat island phenomenon in the Tokyo metropolitan area has spread ever more widely, and it is now too wide to treat as a single regional phenomenon. In this paper, the authors have analyzed the climate on an urban scale in summer, and compared the regional characteristics of the atmospheric heat balance at the center of Tokyo, an inland satellite city, and a satellite city on the other side of Tokyo Bay, using a computational fluid dynamics (CFD) simulation. From the results of the analysis, the authors quantitatively demonstrate the mechanism of diurnal change in air temperature and absolute humidity in these areas, focusing on the heat balance. While the sea breeze prevents the air temperature from increasing in the center of Tokyo, it is less effective as a heat sink in leeward areas, such as the inland satellite city. At the satellite city on the other side of Tokyo Bay, the horizontal wind has some influence on the climate. Additionally, the authors tried to classify the regional characteristic of air temperatures by average air temperature and diurnal range.

KEYWORDS

Numerical Climate Analysis, Heat Island Phenomena, Urban Heat Balance Model, Atmospheric Heat Balance

INTRODUCTION

The heat island phenomenon is observed at many cities (Taha, 1997; Inter-Ministry Coordination Committee to Mitigate Urban Heat Island, 2004). The Tokyo metropolitan area is the most extensively urbanized region in Japan, and extensive sea breezes dominate this area in the afternoon on sunny summer days. The temperature of the sea breeze is lower than that over land, so it mitigates the temperature increase along the bayside area. However, it is thought that these sea breezes also transfer the heat generated from bayside cities to the leeward side. Thus, the heat island phenomena in the Tokyo metropolitan area in summer have spread ever more widely, with differing characteristics per region. These phenomena are clearly evident from observation data (Fujibe, 1997; Mikami, 2000) and numerical simulation data (Fujino, 1993). Therefore, in order to implement effective countermeasures against the heat island phenomena, it is important to understand quantitatively the mechanism of air temperature increase in each region.

The authors have proposed a new concept "Urban Heat Balance Model" (Murakami, 2003). Figure 1 illustrates the concept of this model. In this model, an arbitrary domain in the urban area is regarded as the Control Volume (CV) to comprehensively calculate the heat balance. This model is composed of incoming and outgoing heat fluxes through all virtual surfaces of the CV (Appendix A), anthropogenic heat emission, and heat storage in the CV as shown in Fig. 2. These heat fluxes are calculated from numerical data provided by CFD analyses of a mesoscale climate. Thus, the Urban Heat Balance

[†] Corresponding Author: Tel: +81 3 5452 6435, Fax: +81 3 5452 6432

E-mail address: ooka@iis.u-tokyo.ac.jp

Model provides a means of analyzing urban thermal environments, focused on heat balance.

In this study, the authors analyzed the atmospheric heat balance at the center of Tokyo, a satellite city on the other side of Tokyo Bay, and an inland satellite city. The mechanism of diurnal change in air temperature and absolute humidity in these areas is demonstrated quantitatively with respect to the heat balance of the atmosphere.

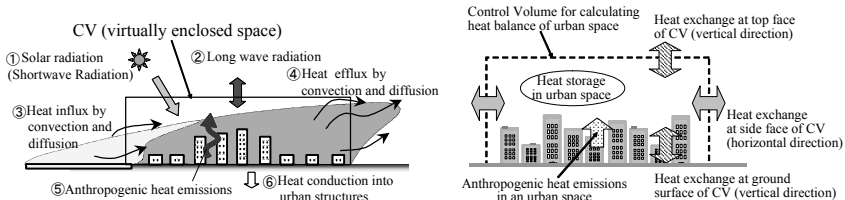


Fig. 1 Concept of the Urban Heat Balance Model Fig. 2 Each components of Urban Heat Balance Model

OUTLINE OF ANALYSIS

Computational domains and grid arrangements

The computational domains are shown in Fig. 3 and Table 1. In this study, sea breeze is focused on as one of the crucial environmental components. Because the sea breeze is formed by large-scale geographical conditions, the nested grid technique is used. The whole computational domain (Grid 1) is nested into two sub-domains; Grids 2 and 3. The vertical direction, Z axis, in all Grids is equally divided from the ground surface up to an altitude of 9.6 km with 49 non-uniform meshes. Moreover, the subterranean layer from the ground surface to a depth of 1 m is divided into 5 non-uniform meshes.

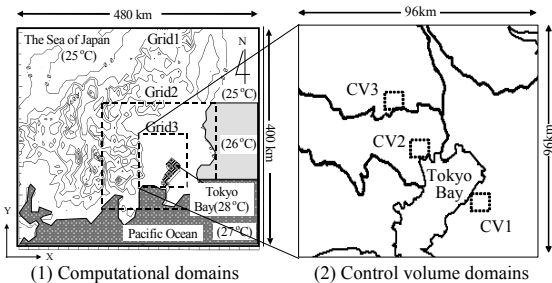


Fig. 3 Computational and control volume domain

Table 1 Computational domains and grid arrangements

Computational Domain	Mesh Number	Horizontal Mesh
(x [km]×y [km] ×z [km])		Size [km]
Grid 1	60 × 50 × 49	8
Grid 2	58 × 50 × 49	4
Grid 3	48 × 48 × 49	2

Numerical climate model

In this study, the authors use a numerical climate model with equations that use hydrostatic approximation. As a turbulence closure model, the Mellor-Yamada model (level 2.5) is used (Mellor and

Yamada, 1974, 1982; Yamada and Bunker, 1989). This model is regarded as a simplified Algebraic Second-moment Closure Model (ASM) as used in engineering. All computations are carried out by a Software Platform for urban heat island analysis (Murakami et al., 2000). The accuracy of the numerical prediction in the above results had been confirmed by Mochida et al. (1997) and Murakami et al. (2000).

Initial and boundary conditions

The initial conditions are shown in Table 2. The target period is a typical sunny day in summer. The simulation starts from 6:00 a.m. with a time integration of 42 hours. The results obtained from 0:00 a.m. (18 hours after the calculation starts) to 0:00 a.m. on the next day (42 hours after the calculation starts) are used to evaluate the heat balance of the atmosphere. The topography and present land cover are used to specify the boundary conditions of the ground surface. The ground surface is classified into 12 types of land cover (Table 4) using a numerical database (Digital National Land Information; 1999). Ground surface temperature is estimated by the heat energy balance at the ground. Boundary conditions for transport equations of momentum, potential temperature, and specific humidity are provided based on the similarity theory of Monin-Obukhov. At the top of the computational domain, the wind direction and velocity are fixed at the initial condition. Anthropogenic heat emission is assumed as sensible heat. It includes wasting heat from automobiles, factories, building air-conditioning systems and so on. The details of the initial and boundary conditions are as given by Mochida et al. (1997) and Murakami et al. (2000).

Target regions for comparing atmospheric heat balance

The CVs are located as shown in Fig. 3 and Table 3. The domain of each CV is 6 km (north-south direction) × 6 km (east-west direction), and 120 m (vertical [Z] direction) (Appendix B). CV1 can be considered to demonstrate that the influence of the temperature increase by urbanization is smaller than that of the other areas (Appendix C). The land-cover ratio of each CV is shown in Table 4. The ratio of high moisture availability (rice paddies, farmland and forests) in CV1 is the largest of the three CVs. The ratio of artificial cover (buildings and paved roads) in CV2 is the largest of the three CVs.

Initial potential temperature near the ground surface	26.0°C
Potential temperature gradient	5.0K/km (0~5km) 4.0K/km (5~9.6km)
Geostrophic wind (wind direction)	2.0m/s (S)
Relative humidity near the surface	70%
Precipitable water	1.3cm
Temperature at the sea surface (fixed)	Tokyo Bay: 28 °C Pacific Ocean: 25-27 °C The Sea of Japan sea: 25 °C
Cloud cover ratio (fixed)	30%

No.	Target region
CV1	Ichihara City, the satellite city on the other side of Tokyo Bay
CV2	Chiyoda, Chuo and Minato Ward, the center of Tokyo, bay side of Tokyo Bay
CV3	Saitama, Asaka and Toda City, the inland satellite city

Table 4 Surface parameter and land-covering ratio for each CV

Classification	Surface parameter					Land-cover ratios of each CV [%]		
	Moisture availability [-]	Albedo [-]	Roughness length z_0 [m]	Thermal diffusion coefficient [$\times 10^6 \text{m}^2/\text{s}$]	Heat capacity [$\times 10^6 \text{J/m}^3\text{K}$]	CV1	CV2	CV3
Rice paddies	0.50	0.20	0.05	0.67	3.00	22.35	0.01	4.84
Farmland	0.30	0.10	0.01	0.40	2.00	6.63	0.00	9.85
Orchard 1	0.30	0.20	1.00	0.30	1.80	1.54	0.00	0.12
Orchard 2	0.30	0.20	0.50	0.30	1.80	0.02	0.00	0.32
Forests	0.30	0.15	2.00	0.15	2.00	9.66	0.03	2.53
Vacant land	0.30	0.20	0.01	1.40	1.90	3.33	0.00	3.88
Buildings	0.00	0.10	1.00	2.30	2.10	36.92	73.79	46.42
Paved roads	0.00	0.10	0.01	2.00	2.00	2.01	10.14	2.97
Other land	0.30	0.10	0.01	1.00	2.00	11.20	9.88	14.10
River site	1.00	0.03	0.001	0.15	4.20	6.34	6.15	14.97
Coast	0.60	0.25	0.005	0.74	2.90	0.00	0.00	0.00

NUMERICAL ANALYSIS RESULTS

Horizontal distributions of various physical quantities

Fig. 4 illustrates the horizontal distributions of wind velocity, air temperature and absolute humidity at a height of 10 m at 2:00 p.m. The flow pattern of sea breezes in the afternoon is accurately reproduced. As more wind passes from the bay side towards the inland area of the Kanto Plain, the wind becomes weaker. Around CV1, the wind direction is along the coast, without forming a sea breeze. However, it must be noted that large-scale sea breezes from the Pacific Ocean to the inland areas of the Kanto Plain dominates overall in Grid 3. The high temperature area spreads from around CV2 to around CV3, with the maximum temperature found around CV3, as shown in Fig. 4(2). The absolute humidity around CV2 and CV3 is lower than that in the surrounding areas, as shown in Fig. 4 (3).

Vertical profiles of various physical quantities

Figs. 5 and 6 compare the vertical profiles of various physical quantities at representative points in each CV from ground level to altitudes of 2,000 m and 200 m at 2:00 p.m. In CV2, the vertical component of the wind indicates a positive value of about 0.02 m/s, which equates to an upward flow, from ground level to an altitude of 400 m as shown in Fig. 5(1). The values above an altitude of 400m become negative, equating to a downward flow. In CV3, the altitude of positive signs is increased to 1,400 m, and the maximum value increases to about 0.2 m/s compared to CV2. Moreover, that maximum value of vertical turbulent diffusivity coefficient in CV3 is the largest of the three CVs as shown in Fig. 5(2). This indicates a significant value to an altitude of 1,400 m. The differences between CV2 and CV3 depend on buoyancy. The temperature near the ground surface in CV3 is the highest of the three CVs, and thus the convection caused by the buoyancy becomes more active than that in the other CVs. As a result, the height of the convection mixed layer in CV3, which demonstrates constant temperature and absolute humidity values, is the highest of the three CVs (Fig. 5(3)(4)).

Diurnal variations of various physical quantities

Fig. 7 compares the diurnal variations in the horizontal wind velocity, air temperature and absolute humidity in each CV. The wind velocity in each CV increases during the day. This is caused by the large-scale sea breeze. The value in CV2 increases at about 10:00 a.m. Moreover, the sea breeze reaches CV3 later than CV2. Upward flow due to a convective mixed layer prevents the sea breeze from moving inland from 10:00 a.m. to 1:00 p.m. (Gamo, 1988). Air temperature (Fig. 7 (2)) in CV1 is the lowest throughout the day. Even though CV2 is veiled with the largest artificial land cover (c.f. Table

4), the maximum daytime temperature is not the highest of the three CVs. As for absolute humidity (Fig. 7 (3)), the value for CV1 reaches its first maximum at about 8:00 a.m. and a second peak at about 6:00 p.m. The value from noon to 3:00 p.m. in CV3 is the smallest of the three CVs. The reasons are considered in next chapter.

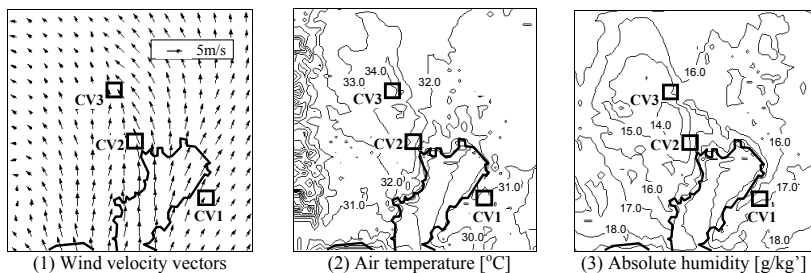


Fig. 4 Horizontal distributions of various physical quantities (Grid 3, at a height of 10m, 2:00 p.m.)

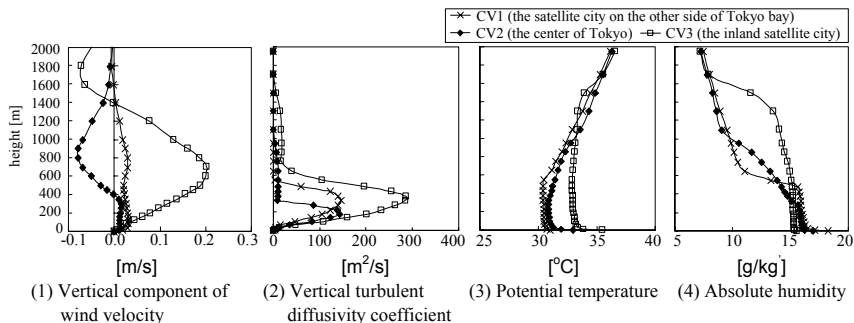


Fig. 5 Vertical profiles of various physical quantities (from ground level to altitude of 2,000m, 2:00 p.m.)

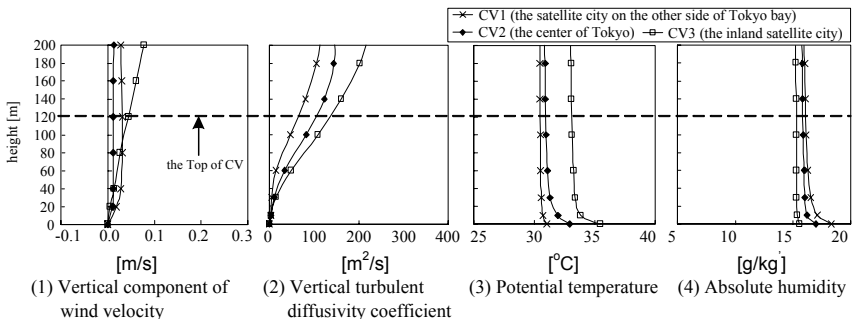
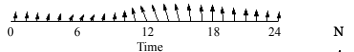


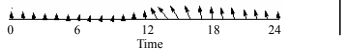
Fig. 6 Vertical profiles of various physical quantities (from ground level to altitude of 200m, 2:00 p.m.)



(a) CV1 (the satellite city on the other side of Tokyo bay)

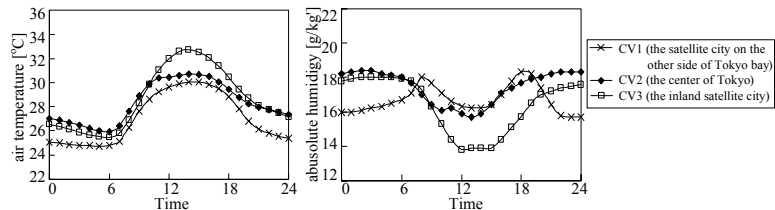


(b) CV2 (the center of Tokyo)



(c) CV3 (the inland satellite city)

(1) Horizontal wind velocity vectors
(at a representative point, at a height of 10 m)



(2) Air temperature [°C]
(spatial average of CV)

(3) Absolute humidity [g/kg']
(spatial average of CV)

Fig. 7 Diurnal variations in the horizontal wind velocity, air temperature and absolute humidity

ANALYSIS OF ATMOSPHERIC HEAT BALANCE BASED ON THE URBAN HEAT BALANCE MODEL

Comparison of sensible heat

Sensible heat transferred through each face

Figs. 8, 9 and 10 present the calculated results based on the Urban Heat Balance Model (Appendix A). Fig. 8 shows the diurnal variations in the hourly integration value of sensible heat transferred through each face and anthropogenic heat emission (c.f. Fig. 2). Fig. 9 shows the diurnal variations in the sensible heat storage and release for each direction (vertical, East-to-West, North-to-South) by adding up the heat transferred through each face in Fig. 8. The anthropogenic heat emission is internal heat generation of a CV, so the value in Fig. 9 is the same as Fig. 8. In Figs. 8 and 12, positive and negative signs indicate heat influx and efflux from a CV respectively. In Figs. 9, 10, 13 and 14, positive and negative signs indicate the heat storage and release of a CV.

(1) CV1 (satellite city on the other side of Tokyo Bay)

Less sensible heat is transferred through each face than the other two CVs (Fig. 8(1)). In terms of the total value of each direction (Fig. 9(1)), the heat storage caused by heat influx in the vertical direction is larger than the other components. This contributes to the temperature increase during the morning. On the other hand, the heat release caused by heat efflux in the North-South direction (Fig. 9(1)) prevents the temperature from increasing.

(2) CV2 (center of Tokyo)

Sensible heat influx is the largest of the three CVs (Fig. 8(2)). This is caused by heat influx from the solar-heated ground surface and anthropogenic heat emission. Consequently, huge heat storage is generated during the day in CV2 (Fig. 9(2)). However, the air temperature in CV2 is lower than in CV3

(c.f. Fig. 7(2)). The reason is considered to be as follows. The total sensible heat at the side face (North-South and East-West direction) is negative. This heat release indicates advection of the sea breeze whose temperature is less than that in CV2. As a result, the overall sensible heat storage for CV2 does not become as massive.

(3) CV3 (inland satellite city)

The total value in the vertical direction is positive from 7:00 a.m. to noon (Fig. 9(2)). The component in the North-South direction demonstrates heat release from this CV. However, the absolute value is much smaller than that in CV2. This is because CV3 is located on leeward of CV2. The sea breeze is weakened by frictional stress from the ground surface, and heated at the center of Tokyo. Furthermore, even if the sea breeze reaches CV3, it has less potential to prevent a temperature increase as a heat sink. Eventually, the total heat storage in CV3 is larger than that in CV2 in Fig. 9 (3).

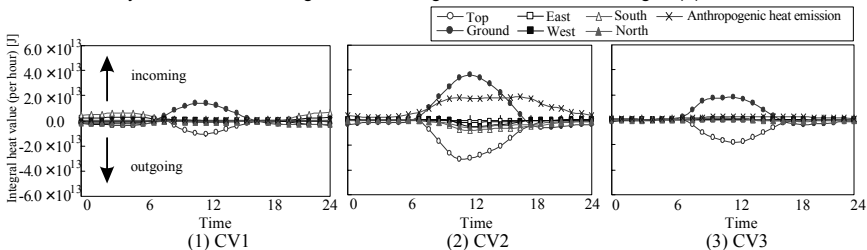


Fig. 8 Diurnal variations in the sensible heat transferred through each face [J] (Appendix A)

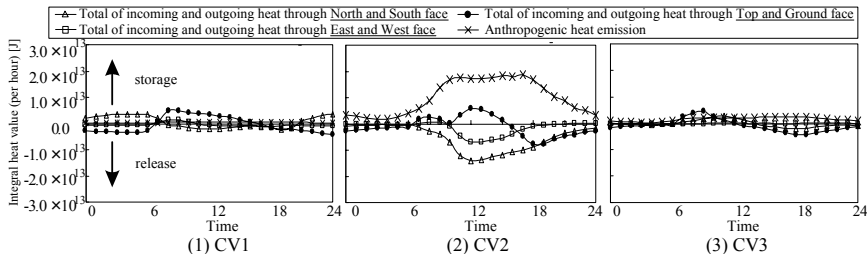


Fig. 9 Diurnal variations in the sensible heat storage and release for each direction (North-South, East-West, Vertical) and anthropogenic heat emissions [J] (Appendix A)

Sensible heat budget for each component of heat transfer

Fig. 10 shows the diurnal variations in sensible heat budget for each component of heat transfer. Here, these components are classified into advection, turbulent diffusion and anthropogenic heat emission. The heat budget for advection and turbulent diffusion are the integral of all surfaces of the CV.

In CV1 and CV2, the advection demonstrate negative values during the day. In particular, the absolute value in CV2 is the largest of the three CVs. This indicates that the sea breeze from Tokyo Bay has a much more significant impact as a heat sink in CV2.

In the heat budget for turbulence diffusion, the diurnal variation is similar to the total value in the vertical direction in each CV (c.f. Fig. 9). In CV1 and CV3, the maximum peak for heat storage is at about 8:00 a.m. In CV2, heat storage by turbulent diffusion increases rapidly from about 11:00 a.m., and reaches a maximum at about noon. This peak for CV2 happens at almost the same time as the amount of heat release by advection grows to its maximum peak. In other words, the large temperature difference

between the atmosphere and ground surface caused by the influx of sea breeze promotes increasing heat flux from the ground surface into the atmosphere.

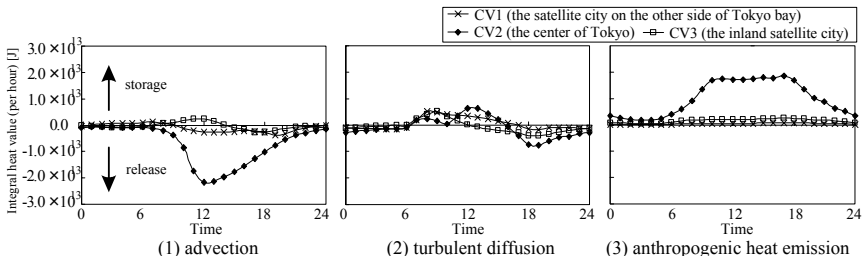


Fig.10 Diurnal variations in sensible heat budget for advection, turbulent diffusion and anthropogenic heat emission (Appendix A)

Characteristics of diurnal variation in air temperature for each area

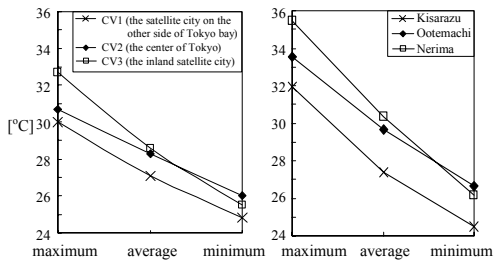
Table 5 shows the maximum, average and minimum temperatures and diurnal range of air temperatures in each CV obtained from Fig. 7(2). The characteristics of its diurnal variation in each area are classified based on the following assumptions. In CV1, a temperature increase caused by urbanization is not found, and the average value and diurnal range of temperature is at normal level. Fig. 11 compares the simulation data in this study with the observed data from a typical fine midsummer's day by the Japan Meteorological Agency. This observation data from July 28 – 31 in 1992 is selected based on the research achievements by Suzuki et al. (2001), and the nearest data point is used. Since the value of the simulation is the spatial average of a CV, it cannot be compared directly with observation data. Therefore, the authors only compare the trends for regional characteristics.

The temperature level in CV2 and CV3 is higher than that in CV1. In CV2, the anthropogenic heat emission and heat storage in urban structures accelerate an increase in the minimum temperature, and the sea breeze prevents an increase in the maximum temperature. Therefore, the diurnal range of air temperature in CV2 is narrower than those in the other CVs. The minimum temperature in CV3 is lower than that in CV2. However, the maximum temperature in CV3 is higher than that in CV2. The above trends show good agreement with observation data (Fig. 11(2)). Although these trends have already been reported by Fujino (1993), Fujibe (1998), and Mikami (2000), these mechanisms can now be quantitatively explained by the Urban Heat Balance Model.

Additionally, it is possible that more effective countermeasures against urban heat island can be proposed from the viewpoint of each regional characteristic. Firstly, it is important that CV2 can reduce the daily minimum temperature, and an urban configuration is built that allows for efficient introduction of sea breeze. Secondly, reducing heat fluxes from the ground surface is significant for CV3 to prevent temperature increases during the day. Countermeasures include planting more greenery, cool roofing and so on.

Table 5 Trend of air temperature in each CV

CV	Region	Maximum	Average	Minimum	Diurnal	Characteristic of temp.	
		Temp.	Temp.	Temp.		range	Temp.
		[°C]	[°C]	[°C]	[°C]	level	range
CV1	the satellite city on the other side of Tokyo Bay	30.0	27.1	24.8	5.2	Standard	Standard
CV2	The center of Tokyo	30.7	28.3	26.0	4.7	High	Narrow
CV3	The inland satellite city	32.7	28.6	25.5	7.2	High	Wide



(1) CFD results (spatial average) (2) Observation data (July 28 -31,1992)
 Fig. 11 Comparison of CFD results and observation data

Comparison of latent heat

Latent heat transferred through each face

Figs. 12 and 13 show the results of latent heat based on the same classification in Figs. 8 and 9.

(1) CV1 (satellite city on the other side of Tokyo Bay)

Because there is much higher evaporative land cover, both influx from the ground surface and efflux from the top face show the largest value of the three CVs (Fig. 12(1)). Though latent heat influx from the ground surface increases from 6:00 to 8:00 a.m., the efflux is not as large under stable atmosphere at this time. Accordingly, the total heat value in the vertical direction shows the maximum value at 8:00 a.m. (Fig. 13(1)). After that, the North-South direction increases and reaches a maximum peak at 5:00 p.m.

(2) CV2 (center of Tokyo)

Most of the heat incoming from the ground surface and the south face flow out from the top face as shown in Figs. 12(2), 13(2). The positive value at the south face is caused by the sea breeze. From the above results, latent heat is mainly supplied in the North-South direction and discharged mainly in the vertical direction as shown in Fig. 13(2).

(3) CV3 (inland satellite city)

The total heat in the North-South direction changes from a positive value in CV2 to a negative value in CV3 during the day (Fig. 13(2)(3)). This change is caused by the decreased humidity of incoming air in CV3, because of the latent heat outgoing from the top face around CV2.

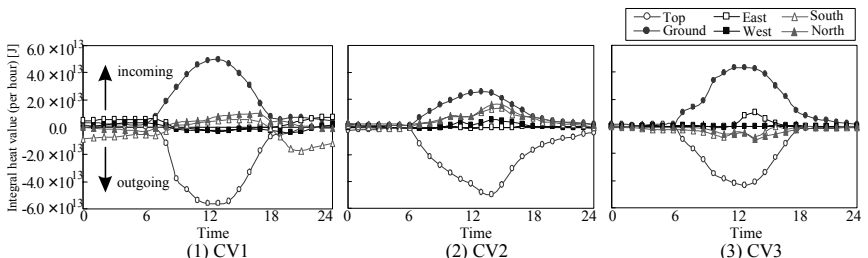


Fig. 12 Diurnal variations in the latent heat transferred through each face [J] (Appendix A)

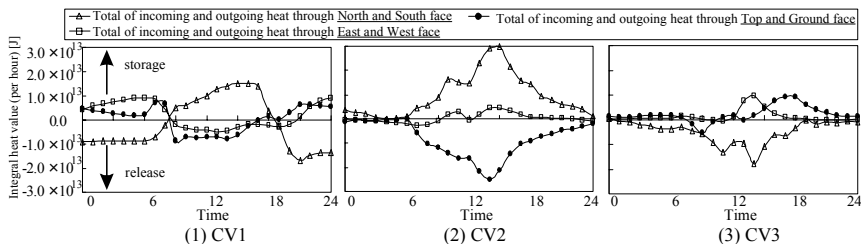


Fig. 13 Diurnal variations in the latent heat storage and release for each direction (Vertical, North-South, East-West), [J] (Appendix A)

Latent heat budget for each component of heat transfer

Fig. 14 indicates the diurnal variations in the latent heat budget for advection and turbulent diffusion. As with the case of the sensible heat budget, the latent heat budget for advection represents the total heat in the horizontal direction, and turbulent diffusion represents the vertical direction. The absolute humidity has two peaks in CV1 (c.f. Fig. 7(3)). The first peak at 8:00 a.m. is mainly caused by latent heat storage by turbulent diffusion in the vertical direction, and the second peak at 6:00 p.m. is mainly caused by advection in the North-South direction. In CV2, the absolute value of latent heat storage by advection and release by turbulent diffusion are much larger than in the other CVs. The reason for this heat release is that the value of turbulent diffusivity coefficient at the top face (altitude of 120 m) is comparatively large as shown in Fig. 6 (2). Fig. 7 (3) shows that the absolute humidity during the day in CV3 is the smallest of the three CVs. The reason is considered to be that both components for advection and turbulent diffusion release latent heat from CV3 in the morning.

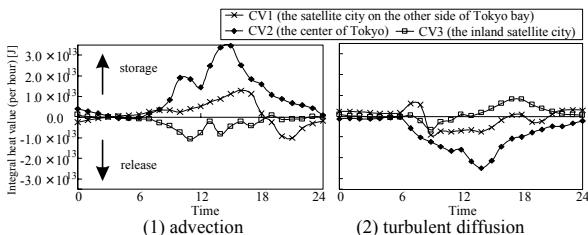


Fig.14 Diurnal variations in latent heat budget for advection and turbulent diffusion (Appendix A)

CONCLUSIONS

- (1) The urban scale climate in summer is analyzed based on CFD simulation. The authors compared the regional characteristics of the atmospheric heat balance at the center of Tokyo, a satellite city on the other side of Tokyo Bay, and an inland satellite city, using the Urban Heat Balance Model based on the concept of Control Volume. From the results, the mechanism of diurnal variation in the air temperature and absolute humidity is quantitatively demonstrated.
- (2) In this study, the regional characteristics of diurnal variation in air temperature for each area show good agreement with the observed data. Moreover, the authors tried to classify the regional characteristics of air temperature from the viewpoints of sensible heat balance and diurnal variation in the air temperature. These results indicate the most suitable countermeasures against urban heat island phenomena in each region.
- (3) At the center of Tokyo, the sea breeze from Tokyo Bay has a great impact. It prevents the

temperature from increasing and absolute humidity from decreasing during the day.

- (4) At the satellite city on the other side of Tokyo Bay, the horizontal wind has some influence on the climate in this area. In particular, sensible heat release caused by heat efflux in the North-South direction prevents a temperature increase.
- (5) Because sea breezes pass through the center of Tokyo, airflow by the side face has less impact as a heat source or a heat sink in the inland satellite city. As a result, vertical heat transfer dominates the climate on this area.

This paper has shown how to prepare a paper for submission to IAQVEC 2007 Conference. Good luck with your paper and look forward to meeting you in Sendai!

Appendix A

To consider the atmospheric heat gain, it is useful to analyze heat influx and efflux at each CV surface as shown in Figs. 8 and 9. Therefore, the authors defined the components of heat gain corresponding to advection and turbulent diffusion at each CV surface as shown in Equation (1), (3). Fig. 15 illustrates the definition of heat flux at a CV boundary surface. Heat gains at dS_i are calculated using parameters on the figure, which are predicted by CFD analysis. Here, the component of heat gain corresponding to advection at dS_i is defined as follows.

$$dQ_{AD} = c_p \rho_i u_i (\theta_i - \theta_A) dS_i \quad (1)$$

Equation (1) differs from the normal expression of advection, due to introduction of the reference value and evaluating one particular surface. If dQ_{AD} is integrated on all CV surfaces, the result is the normal expression of advection as shown below.

$$\begin{aligned} Q_{AD} &= c_p \rho \int u_i (\theta_i - \theta_A) dS_i \\ &= c_p \rho \left(\int u_i \theta_i dS_i - \theta_A \int u_i dS_i \right) \\ &= c_p \rho \int u_i \theta_i dS_i \end{aligned} \quad (2)$$

The component of heat gain corresponding to turbulent diffusion at dS_i is defined as follows.

$$dQ_{DIFF} = c_p \rho K_i \left(\frac{d\theta}{dx} \right)_i dS_i \quad (3)$$

Moreover, the latent heat is defined as well as sensible heat by using absolute humidity q_i [g/kg] at dS_i and the spatial average absolute humidity q_A [g/kg] within the CV. Figs. 8, 9, 12 and 13 are the results based on Equation (1) or (3), and Figs. 10 and 14 are the results based on Equation (2).

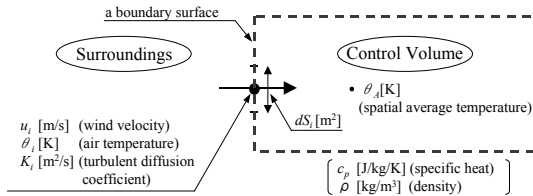


Fig. 15 Definition of sensible heat fluxes at boundary surface

Appendix B

There are many ideas to decide the height of the CV. In this study, the authors set an optimum height to evaluate urban heat balance structure based on many case studies into countermeasures. Firstly, the height is set above the surface boundary layer and under the convective mixed layer. Secondly,

because buildings have a significant influence on urban climates, a top surface is required to cover most buildings in an urban space. Based on the above investigation, the authors set the height of the CV as an altitude of 120 m.

Appendix C

It is difficult to judge the degree of warming due to urbanization. Fujibe (1997) used air temperature from the time before the temperature increase due to urbanization based on historical observation data. Mochida et al. (1999) and Ichinose (2003) compared historical air temperatures obtained by a numerical simulation. Moreover, Mochida et al. (1997) used simulation results assumed the land cover across the whole of the computational domain to be greenery. In this study, from a viewpoint of geographical condition, a satellite city on the other side of Tokyo Bay is chosen. Although there is artificial land cover, the ratio is not as high as the central part of the urban area. Furthermore, the metropolitan area does not exist at the windward during summer sea breezes.

REFERENCES

1. Digital national land information, Geographical Survey Institute, Ministry of Land, Infrastructure and Transport, 1999
2. Fujibe, F., 1997, Time-of-the-Day Dependence of Long-Term Temperature Changes at Urban Meteorological Stations in Japan, *Journal of the Meteorological Society of Japan*, Vol.75, No.6, 1041-1051
3. Fujibe, F., 1998, An Increasing Trend of Extremely Hot Days in the Inland of the Kanto Plain and its Relation to Urban Effects, *TENKI*, Vol.45, No.8, 643-653
4. Fujino, T. et al., 1993, Characteristics of Suburban Heat Island with an Example of Northern Part of Tokyo, *Research Report of Dept. Civil & Environmental Eng. Saitama Univ.*, Vol.23, 127-134
5. Gamo, M., 1988, Hourly Change of Advance of the Sea-breeze Front over Kanto Area, *Kogai*, 23, 37-46 (in Japanese with English abstract)
6. Taha, H, 1997, Urban climates and heat islands: albedo, evapotranspiration, and anthropogenic heat, *Energy and buildings* 25, 99-103
7. Inter-Ministry Coordination Committee to Mitigate Urban Heat Island, 2004, *OUTLINE OF THE POLICY FRAMEWORK TO REDUCE URBAN HEAT ISLAND EFFECTS*
8. Ichinose, T., 2003, Regional warming related to land use change during recent 135 years in japan, *Journal of Global Environment Engineering*, Vol.9, 19-39
9. Mellor, G.L., Yamada, T., 1974, A Hierarchy of Turbulence Closure Models for Planetary Boundary layer, *J of Applied Meteorology*, Vol.13, No.7, 1791-1806.
10. Mellor, G.L., Yamada T., 1982, Development of a Turbulence Closure Model for Geophysical Fluid Problem, *Rev. Geophys. Space Phys.*, Vol.20, No.4, 851-875
11. Mochida, A. et al., 1997, CFD analysis of mesoscale climate in the Greater Tokyo area, *Journal of Wind Engineering and Industrial Aerodynamics* 67&68 pp. 459-477
12. Mochida, A. et al., 1999, CFD Study on Urban Climate in Tokyo - Effects of urbanization on climatic change -, 10th International Conference on Wind Engineering, Copenhagen, Denmark, pp.1307-1214
13. Mikami, T. et al., 2000, Investigation of urban heat islands in Tokyo Metropolis based on the ground monitoring system. *Biometeorology and urban climatology at the turn of the millennium*, WMO/TD, N.1026, pp491-495.
14. Murakami, S. et al., 2000, Software Platform for the total analysis of wind climate and urban heat island, -integration of CWE simulations from human scale to urban scale-, *CWE2000*, University of Birmingham, UK
15. Murakami, S. et al., 2003, 11th International Con. on Wind Engineering, Evaluation of the Impacts

of Urban Tree Planting in Tokyo Based on Urban Heat Balance Model

16. Suzuki, T. et al, 2001, Extracting Diurnal Temperature Changing Patterns of Tokyo in Mid-summer- Grasping Heat Island Phenomena by means of Statistical Methods - , TENKI, Vol. 48, No. 6, pp.383-391 (in Japanese with English abstract)
17. Yamada, T., Bunker, S., 1989, A Numerical Model Study of Nocturnal Drainage Flows with Strong Wind and Temperature Gradients, Journal of Applied Meteorology, Vol.28, 545-554